

# High-dimensional maximum-entropy phase space tomography using normalizing flows

Austin Hoover\*

Oak Ridge National Laboratory, Oak Ridge, Tennessee 37830, USA

Jonathan C. Wong

Institute of Modern Physics, Chinese Academy of Sciences, Lanzhou 730000, China

(Dated: June 10, 2024)

Particle accelerators generate charged particle beams with tailored distributions in six-dimensional (6D) position-momentum space (phase space). Knowledge of the phase space distribution enables model-based beam optimization and control. In the absence of direct measurements, the distribution must be tomographically reconstructed from its projections. In this paper, we highlight that such problems can be severely underdetermined and that entropy maximization is the most conservative solution strategy. We leverage *normalizing flows*—invertible generative models—to extend maximum-entropy tomography to 6D phase space and perform numerical experiments to validate the model performance. Our numerical experiments demonstrate that flow-based entropy estimates are consistent with 2D maximum-entropy solutions and that normalizing flows can fit complex 6D phase space distributions to large measurement sets in reasonable time.

## I. INTRODUCTION

Accelerators generate charged particle beams with tailored distributions in position-momentum space (phase space). Measuring the phase space distribution enables model-based beam optimization and control, but such measurements are challenging when the phase space is high-dimensional. If direct measurements [1–3] are unavailable, the distribution must be tomographically reconstructed from its projections. Fig. 1 shows a typical setup, where each projection corresponds to the beam’s spatial distribution after transport through an accelerator lattice (a series of electromagnetic focusing elements, such as dipole or quadrupole magnets). In the most challenging versions of the problem, we face a 4D or 6D reconstruction from 1D or 2D projections and (potentially) nonlinear transformations [4–12].

It is possible for 6D reconstructions to be severely ill-posed. Since the measured dimension is fixed, the set of feasible distributions—those consistent with the measurements—may proliferate with the phase space dimension. The total number of views can be limited to tens, compared to hundreds in industrial or medical applications. We generally do not know the information-maximizing set of 6D phase space transformations under given measurement conditions, and accelerator constraints place many transformations out of reach. And we do not know the level to which modeling or measurement errors propagate through the 6D reconstruction.

Entropy maximization is a conservative approach to ill-posed inverse problems and is thus well suited to high-dimensional tomography.<sup>1</sup> In this paper, we leverage

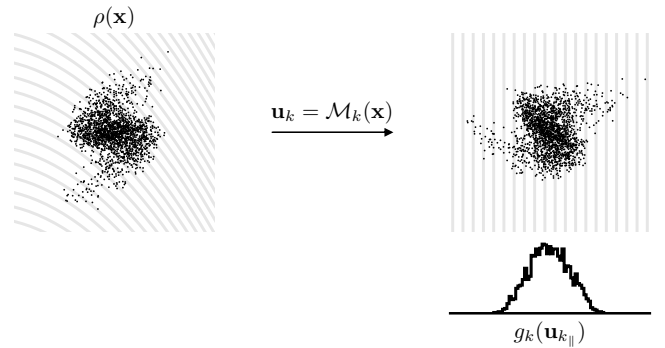


FIG. 1. Generic phase space tomography setup. The  $n$ -dimensional phase space distribution  $\rho(\mathbf{x})$  travels through an accelerator lattice—a series of electromagnetic focusing elements—represented by a symplectic mapping  $\mathbf{u}_k = \mathcal{M}_k(\mathbf{x})$ . We measure the  $m$ -dimensional projections  $g(\mathbf{u}_{k||})$  in the transformed space and use this data to reconstruct  $\rho(\mathbf{x})$ . If the lattice contains nonlinear elements, the projections correspond to curved integration surfaces in the original phase space.

*normalizing flows*—invertible generative models—to extend maximum-entropy tomography to 6D phase space. Our approach is a straightforward merger of two previous studies. Loaiza-Ganem, Gao, and Cunningham [16], first proposed the use of flows for entropy maximization subject to statistical moment constraints; we incorporate projection constraints using the differentiable physics simulations and projected density estimation proposed by Roussel et al. [11] in the Generative Phase Space Reconstruction (GPSR) framework. We refer to the resulting approach as MENT-Flow.

\* hooveram@ornl.gov

<sup>1</sup> Entropy maximization can be derived from self-consistency requirements on any strategy to infer probability distributions from incomplete data [13, 14]. The maximum-entropy distribution has

minimal informational content, eliminating spurious correlations and deviating from prior knowledge only to the extent required by the data [15].

We begin by deriving the form of the  $n$ -dimensional maximum-entropy distribution subject to  $m$ -dimensional projection constraints, extending the 2D and 4D analysis in [7, 17]. We then discuss the shortcomings of existing maximum-entropy tomography algorithms when  $n = 6$  and describe the flow-based solution. Finally, we perform numerical experiments to validate the model's reliability in 2D settings and examine the effects of entropic regularization in 6D tomography.

## II. MAXIMUM ENTROPY TOMOGRAPHY

Let  $\rho(\mathbf{x})$  be a probability distribution over phase space coordinates  $\mathbf{x} \in \mathbb{R}^n$ . We assume the  $k$ th measurement occurs after a symplectic transformation  $\mathcal{M}_k : \mathbb{R}^n \rightarrow \mathbb{R}^n$ . Splitting the transformed coordinates

$$\mathbf{u}_k = \mathcal{M}_k(\mathbf{x}) \quad (1)$$

into a projection axis  $\mathbf{u}_{k\parallel} \in \mathbb{R}^m$  and orthogonal integration axis  $\mathbf{u}_{k\perp} \in \mathbb{R}^{n-m}$ , we write the constraints as

$$g_k(\mathbf{u}_{k\parallel}) - \int \rho(\mathcal{M}_k^{-1}(\mathbf{u}_k)) d\mathbf{u}_{k\perp} = 0 \quad (2)$$

for measured projection  $g_k(\mathbf{u}_{k\parallel})$ . Letting prior  $\rho_*(\mathbf{x})$  encode our knowledge of the distribution in the absence of data, we aim to maximize the entropy

$$H[\rho(\mathbf{x}), \rho_*(\mathbf{x})] = - \int \rho(\mathbf{x}) \log \left( \frac{\rho(\mathbf{x})}{\rho_*(\mathbf{x})} \right) d\mathbf{x}, \quad (3)$$

subject to Eq. (2). We will refer to this problem as an  $n:m$  reconstruction.

We can derive the form of the maximum-entropy distribution from a new functional

$$\Psi[\rho(\mathbf{x}), \rho_*(\mathbf{x}), \{g_k(\mathbf{u}_{k\parallel})\}] = H[\rho(\mathbf{x}), \rho_*(\mathbf{x})] + \sum_k \int \lambda_k(\mathbf{u}_{k\parallel}) \left( g_k(\mathbf{u}_{k\parallel}) - \int \rho(\mathcal{M}_k^{-1}(\mathbf{u}_k)) d\mathbf{u}_{k\perp} \right) d\mathbf{u}_{k\parallel}, \quad (4)$$

where  $\lambda_k(\mathbf{u}_{k\parallel})$  are unknown functions [18]. Enforcing zero variation of  $\Psi$  with respect to  $\rho(\mathbf{x})$  and  $\lambda_k(\mathbf{u}_{k\parallel})$  gives

$$\begin{aligned} \rho(\mathbf{x}) &= \rho_*(\mathbf{x}) \prod_k \exp(\lambda_k(\mathbf{u}_{k\parallel}(\mathbf{x}))) \\ &= \rho_*(\mathbf{x}) \prod_k h_k(\mathbf{u}_{k\parallel}(\mathbf{x})). \end{aligned} \quad (5)$$

The constrained maximum-entropy distribution function at point  $\mathbf{x}$  is the product of two terms: the prior distribution function at  $\mathbf{x}$  and the product of the positive Lagrange functions  $h_k$  evaluated at the corresponding points  $\mathbf{u}_{k\parallel}(\mathbf{x})$  on the measurement axes.<sup>2</sup> Substituting Eq. (5) into Eq. (2) generates a set of coupled nonlinear integral equations from which  $h_k$  are to be solved.

### A. MENT

The MENT algorithm [7, 17–19] leverages a Gauss-Seidel relaxation method to optimize the Lagrange functions in Eq. (5). After initializing the distribution to the prior within the measurement boundaries:

$$h_k(\mathbf{u}_{k\parallel}) = \begin{cases} 1, & \text{if } g_k(\mathbf{u}_{k\parallel}) > 0 \\ 0, & \text{otherwise} \end{cases}. \quad (6)$$

the Lagrange functions are updated as

$$h_k(\mathbf{u}_{k\parallel}) \leftarrow h_k(\mathbf{u}_{k\parallel}) \left( 1 + \omega \left( \frac{g_k(\mathbf{u}_{k\parallel})}{\tilde{g}_k(\mathbf{u}_{k\parallel})} - 1 \right) \right) \quad (7)$$

where

$$\begin{aligned} \tilde{g}_k(\mathbf{u}_{k\parallel}) &= \int \rho_*(\mathcal{M}_k^{-1}(\mathbf{u}_k)) \prod_j h_j(\mathbf{u}_{j\parallel}) d\mathbf{u}_{k\perp} \\ &= h_k(\mathbf{u}_{k\parallel}) \int \rho_*(\mathcal{M}_k^{-1}(\mathbf{u}_k)) \prod_{j \neq k} h_j(\mathbf{u}_{j\parallel}) d\mathbf{u}_{k\perp} \end{aligned} \quad (8)$$

are the simulated projections and  $0 < \omega \leq 1$  is a learning rate [18]. The updates are performed in order ( $k = 1, 2, 3, \dots$ ), and each updated  $h_k$  is immediately used to simulate the next projection. One epoch is completed when all functions are updated. The iterations in Eq. (7) converge [17, 19].

MENT is a powerful tomographic algorithm. Its unique advantage is that it maximizes entropy by design: fitting the data generates an exact solution to the constrained optimization problem. MENT is also efficient (it stores the exact number of parameters needed to define the maximum-entropy distribution and typically converges in a few epochs) and essentially hyperparameter-free. Additionally, although not yet reported in the literature, MENT does not assume the phase space transformations are linear.

We showed above that MENT extends to  $n:m$  tomography. In practice, the value of  $n$  is limited by the integrals required to compute the distribution's projections.

<sup>2</sup> In MENT literature, the Lagrange multipliers/functions often refer to  $\lambda_k$  in Eq. (5), but here we refer to the exponential of  $\lambda_k$ .

Ongoing work aims to demonstrate efficient implementations when  $n = 4$  [7, 20]. Extension to  $n = 6$  may be possible, but it has not been demonstrated, and the runtime may be slow if there are many high-resolution measurements. Additionally, even if the algorithm converged, generating particles would require sampling from

$$L[\rho(\mathbf{x}), \rho_*(\mathbf{x}), \{g_k(\mathbf{u}_{k\parallel})\}] = -H[\rho(\mathbf{x}), \rho_*(\mathbf{x})] + \mu \sum_k D[g_k(\mathbf{u}_{k\parallel}), \tilde{g}_k(\mathbf{u}_{k\parallel})] \quad (9)$$

for an increasing sequence of penalty parameters  $\mu$ . Here,  $D[g_k(\mathbf{u}_{k\parallel}), \tilde{g}_k(\mathbf{u}_{k\parallel})]$  is a non-negative number quantifying the discrepancy between the measured and simulated projections, which we choose to be the Kullback-Leibler (KL) divergence. Although exact solutions may require  $\mu \rightarrow \infty$ , approximate solutions obtained with finite  $\mu$  are often sufficient.<sup>3</sup> This approach requires a parameterization of  $\rho(\mathbf{x})$ . Direct parameterizations require 6D integration or Monte Carlo sampling to compute the distribution's entropy and projections. Indirect parameterizations instead define

$$\mathbf{x} = \mathcal{F}(\mathbf{z}), \quad (10)$$

where  $\mathbf{z}$  is drawn from a base distribution  $\rho_0(\mathbf{z})$  defined in a normalized space. Typically,  $\rho_0(\mathbf{z})$  is an easy-to-sample-from distribution such as a standard Gaussian distribution. Roussel et al. [11] adopted this approach, using a neural network to represent  $\mathcal{F}$  and using differentiable beam dynamics simulations and kernel density estimation to fit the network parameters to projection data. However, it is difficult to maximize the entropy without access to  $\rho(\mathbf{x})$ .<sup>4</sup>

*Normalizing flows* are indirect parameterizations that provide access to the probability density. Flows define

an expensive-to-evaluate 6D distribution function.

## B. MENT-Flow

In the absence of a method to directly optimize the Lagrange functions in Eq. (5), we may try to minimize the loss function

$\mathcal{F} : \mathbb{R}^n \rightarrow \mathbb{R}^n$  as an invertible, differentiable map and compute the density from

$$\log \rho(\mathbf{x}) = \log \rho_0(\mathbf{z}) - \log |\det J_{\mathcal{F}}(\mathbf{z})|, \quad (11)$$

where

$$J_{\mathcal{F}}(\mathbf{z}) = \frac{d\mathcal{F}}{d\mathbf{z}} = \begin{bmatrix} \frac{\partial \mathcal{F}_1}{\partial z_1} & \cdots & \frac{\partial \mathcal{F}_1}{\partial z_n} \\ \vdots & \ddots & \vdots \\ \frac{\partial \mathcal{F}_n}{\partial z_1} & \cdots & \frac{\partial \mathcal{F}_n}{\partial z_n} \end{bmatrix}. \quad (12)$$

is the  $n \times n$  Jacobian matrix of  $\mathcal{F}$ . Given  $N$  flow samples  $\{\mathbf{x}_i\}$ , an unbiased entropy estimate is available: [16]:

$$\begin{aligned} -H[\rho(\mathbf{x}), \rho_*(\mathbf{x})] &= \mathbb{E}_{\rho(\mathbf{x})} [\log \rho(\mathbf{x}) - \log \rho_*(\mathbf{x})] \\ &\approx \frac{1}{N} \sum_{i=1}^N (\log \rho(\mathbf{x}_i) - \log \rho_*(\mathbf{x}_i)) \end{aligned} \quad (13)$$

Since  $\mathcal{F}$  is differentiable, we can maximize the entropy estimate via, e.g., stochastic gradient descent [16]. We call this approach MENT-Flow when combined with differentiable tomographic constraints.

It is not immediately obvious whether flows can learn complex 6D phase space distributions from projection data in reasonable time. Flows are restricted to invertible transformations that preserve the topological features of the base distribution; for example, flows cannot perfectly represent disconnected modes if the base distribution has a single mode [23]. Building complex flows requires layering transformations, either as a series of maps (discrete flows) or a system of differential equations (continuous flows), often leading to large models and expensive training.<sup>5</sup>

We found that Neural Spline Flows (NSF) [25] provide a sufficient blend of speed and power. Each flow layer is an autoregressive transformation of the form

<sup>3</sup> More sophisticated Augmented Lagrangian (AL) methods [16, 21] are available to stabilize the optimization and avoid large penalty parameters, but we did not see significant improvements using AL in our numerical experiments.

<sup>4</sup> Roussel et al. [11] proposed to maximize the *emittance*, or root-mean-square (rms) volume,  $\varepsilon = |\Sigma|^{1/2}$ , where  $\Sigma = \langle \mathbf{x}\mathbf{x}^T \rangle$  is the  $n \times n$  covariance matrix of second order moments, as a proxy for the entropy. For certain distributions, the logarithm of the emittance is proportional to the entropy, but this is not true in general. Like entropy maximization, emittance maximization removes unnecessary linear correlations from the reconstructed distribution. However, it cannot remove nonlinear correlations, as the emittance depends only on second-order moments. Furthermore, the maximum-emittance distribution is not unique. In linear systems, the covariance matrix is typically overdetermined by the tomographic measurements, i.e., all distributions that fit the data have the same emittance. Particle-based entropy estimates based on  $k$  nearest neighbors [22] may perform better.

<sup>5</sup> A relevant example comes from Green, Ting, and Kamdar [24], who used continuous flows for 6D phase space density estimation from measured stellar phase space coordinates; training times ranged from hours to days on a GPU, depending on the distribution complexity, with approximately  $10^4$  particles per batch.

$$z_i \rightarrow \mathcal{F}(z_i; c_i(z_1, \dots, z_{i-1})), \quad (14)$$

where  $\mathbf{z} = [z_1, \dots, z_n]^T$ . Here,  $\mathcal{F}$  is an invertible function conditioned on  $c_i(z_1, \dots, z_{i-1})$ . The conditioner generates a triangular Jacobian whose determinant can be efficiently computed. We implemented the conditioner using a masked neural network [26] and the transformer using rational-quadratic splines [25]. Representational power increases with the number of neural network parameters, the number of knots in the spline transformer, and the number of flow layers. For the composition of  $T$  layers

$$\mathcal{F} = \mathcal{F}_T \circ \mathcal{F}_{T-1} \circ \dots \circ \mathcal{F}_2 \circ \mathcal{F}_1, \quad (15)$$

and transformed coordinates

$$\mathbf{z}_t = \mathcal{F}_t(\mathbf{z}_{t-1}), \quad (16)$$

the Jacobian determinant is available from

$$|J_{\mathcal{F}}(\mathbf{z}_0)| = \prod_{t=1}^T |J_{\mathcal{F}_t}(\mathbf{z}_{t-1})|. \quad (17)$$

MENT-Flow increases the reconstruction model complexity and does not guarantee an exact entropy maximum. However, MENT-Flow scales straightforwardly to  $n$ -dimensional phase space and immediately generates independent and identically distributed samples from the reconstructed distribution.

### III. NUMERICAL EXPERIMENTS

The following numerical experiments demonstrate that MENT-Flow solutions approach MENT solutions in 2D phase space. Subsequent experiments demonstrate that MENT-Flow can fit complicated 6D phase space distributions to large measurement sets in reasonable time and that entropic regularization keeps the reconstruction close to the prior distribution. We tended to use ground-truth distributions without linear interplane correlations and simple transformations rather than realistic accelerator models.<sup>6</sup> We also chose to maximize the entropy relative to a Gaussian prior distribution ( $\rho_*(\mathbf{x})$ ) and used a Gaussian base distribution, making the maximum-entropy flow a linear transformation.<sup>7</sup> All training and analysis code is available in an online repository [27].

<sup>6</sup> Equivalently, we assume we know the covariance matrix  $\Sigma = \langle \mathbf{x}\mathbf{x}^T \rangle = \mathbf{V}\mathbf{V}^T$  and reconstruct the distribution in normalized coordinates  $\mathbf{x}_n = \mathbf{V}^{-1}\mathbf{x}$  by setting  $\mathcal{M}_k \rightarrow \mathcal{M}_k\mathbf{V}$ . The covariance matrix is usually overdetermined by the measurements—for example, three measurements determine the  $2 \times 2$  covariance matrix—so that all distributions that fit the data share the same covariance matrix. In these cases it is reasonable to fit the covariance matrix first.

<sup>7</sup> A Gaussian prior may be a reasonable choice for accelerator applications: the prior has no interplane dependence and can ex-

#### A. 2D reconstructions from 1D projections

Our first experiment tests the model performance in 2:1 phase space tomography. We assume a linear accelerator lattice, composed of drifts and quadrupole magnets, such that a symplectic transfer matrix  $\mathbf{M}$  approximates the dynamics. The transfer matrix can be decomposed as

$$\mathbf{M} = \mathbf{V}(\alpha_2, \beta_2)\mathbf{R}(\mu)\mathbf{V}(\alpha_1, \beta_1)^{-1}, \quad (18)$$

where

$$\mathbf{V}(\alpha, \beta) = \begin{bmatrix} \sqrt{\beta} & 0 \\ -\frac{\alpha}{\sqrt{\beta}} & \frac{1}{\sqrt{\beta}} \end{bmatrix} \quad (19)$$

is a normalization matrix, parameterized by  $\alpha$  and  $\beta$ , and

$$\mathbf{R}(\mu) = \begin{bmatrix} \cos \mu & \sin \mu \\ \sin \mu & \cos \mu \end{bmatrix} \quad (20)$$

is a rotation by the phase advance  $\mu$ . The projection angle, and hence the reconstruction quality, depends only on the phase advance. Various constraints can limit the projection angle range, but we assume the projection angles are evenly spaced over the maximum 180-degree range.

Fig. 2 shows reconstructions from a varying number of projections, comparing MENT, MENT-Flow, and an unregularized neural network (NN). It is clear that maximizing the stochastic estimate in Eq. (13) pushes the distribution's entropy close to its constrained maximum. (Recall that MENT maximizes entropy by construction). Although the MENT solutions are of higher quality, the differences are not visible from afar.

Fig. 2 illustrates that entropy maximization is a conservative approach to the reconstruction problem. All reconstructed features are implied by the data. In contrast, the distributions in the bottom rows fit the data but are unnecessarily complex. Of course, reconstructions from one or two projections are bound to fail, no matter the algorithm, but these cases are still useful because they demonstrate MENT's logical consistency: given only the marginal distributions and an uncorrelated prior distribution, MENT returns the product of the marginals. On the other extreme, with enough data, the feasible distributions will differ only in minor details. MENT shines in intermediate cases where the measurements contain just enough information to constrain the distribution's primary features. For example, the continuous spiral structure develops rapidly with the number of views.

pand to approximate a uniform distribution; (ii) any known elements of the  $n \times n$  covariance matrix can be used to define the Gaussian prior; (iii) beams are typically clustered in phase space and approximately Gaussian at equilibrium; (iv) a Gaussian prior can be used to limit the beam size in dimensions that are weakly constrained by the data; and (v) the relative entropy has a maximum of zero.

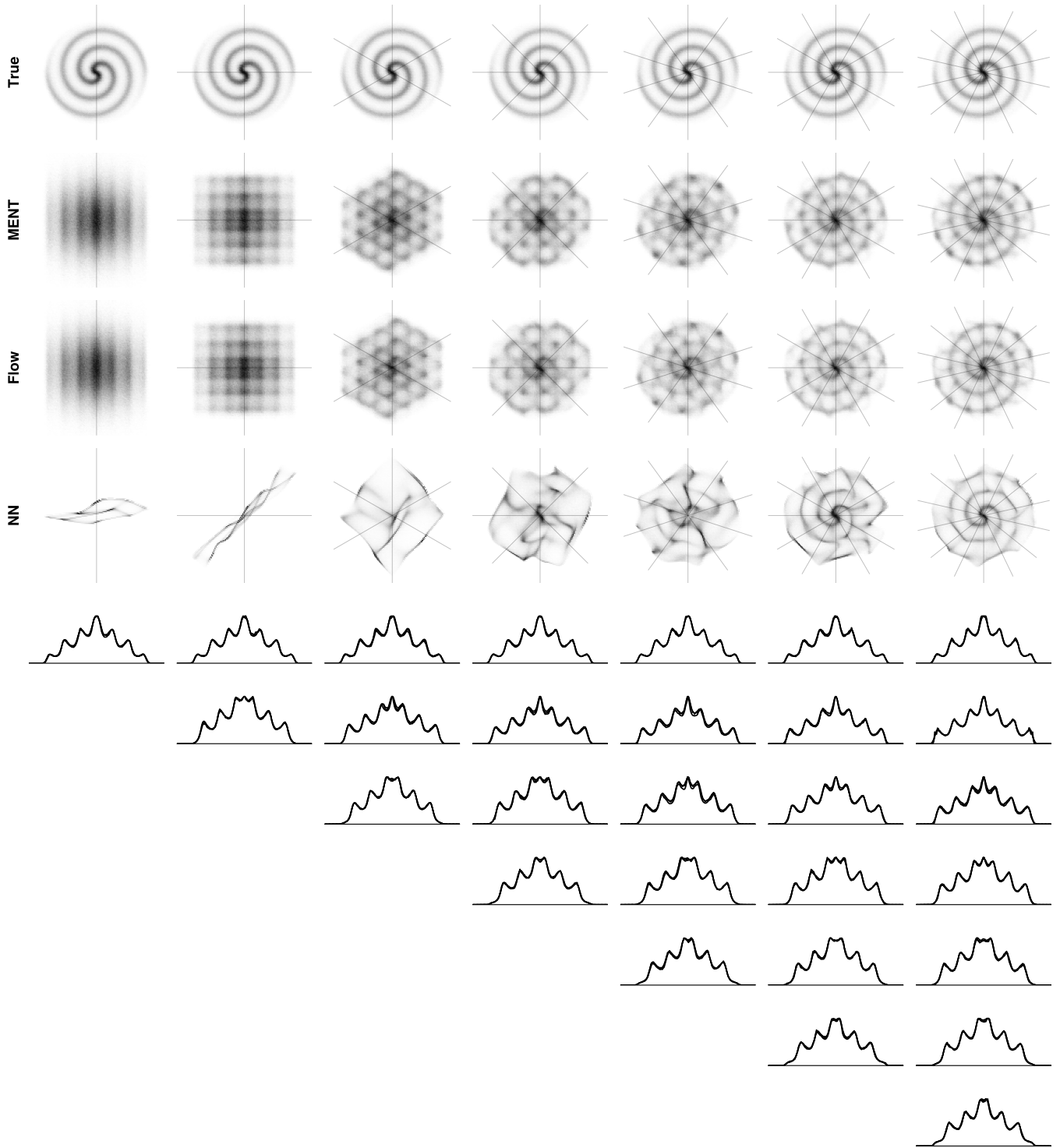


FIG. 2. 2D reconstructions from varying numbers of evenly spaced 1D projections. The top rows plot samples from the true distribution, MENT reconstruction, MENT-Flow reconstruction, and unregularized neural network reconstruction. Faint lines show the evenly spaced projection angles, increasing from 1 on the left column to 7 on the right column. The projections of the four distributions are plotted on the horizontal axes on the bottom rows.

Fig. 2 also illustrates the flow’s capacity to represent complex distributions despite its restriction to invertible transformations. This examples focuses on spiral patterns, which are characteristic of nonlinear dynamics. (Additional examples are included in the supplemental material.) It is important to note that, while our analysis focuses on the beam core, low-density regions can also impact accelerator performance [28]. Flows can struggle to model distribution tails when trained via maximum-likelihood [29]. Our example distribution does not have significant halo and we do not report the agreement at this level, but preliminary studies indicate that the Kullback-Leibler (KL) divergence may enhance dynamic range relative to, i.e., the mean absolute error when fitting the data.

## B. 6D reconstructions from 1D projections

It is more challenging to design and evaluate 6D numerical experiments. *First*, we do not know the information-maximizing set of 6D phase space transformations. In the 2D case, if the transformations are linear, there is a clear connection between a single transformation parameter (the phase advance) and the reconstruction quality. 4D or 6D symplectic transformations require many more parameters [30], and it is unclear which parameters are relevant. Note also that the ideal set of transformations depends on the distribution and on the number of measured dimensions. Here, we restrict our attention to 1D projections, i.e., 6:1 reconstructions, for which we can plausibly obtain the ideal set of linear phase space transformations by generalizing the notion of “projection angle”. A 1D projection axis is defined by a point on the unit  $n$ -sphere; if the distribution is spherically symmetric, we expect the optimal projection axes to be uniformly distributed on the sphere.<sup>8</sup> In the limit of many such projections, the reconstruction will converge to the true distribution [31].

*Second*, there are many possible 6D distributions, and establishing reconstruction accuracy requires high-dimensional visualization or statistical distance metrics. As described shortly, we selected distributions with clear high-dimensional structure and leveraged complete sets of pairwise projections and limited sets of partial projections, i.e., projections of slices, to facilitate the visualization task.

*Third*, we cannot determine the distance from the reconstructed distribution to the true maximum-entropy distribution without an analytic solution. We point to Fig. 2 as evidence that the flow’s entropy estimate can approximate the true entropy, and we continue to train an unregularized neural network on the same data to show that additional solutions can exist far from our prior.

<sup>8</sup> It is unclear what “evenly spaced projection angles” correspond to when the integration planes have dimension  $n - 2$ .

Our first high-dimensional experiment, shown in Figs. 3-4, reconstructs a seven-mode Gaussian mixture distribution from 25, then 100 random 1D projections. This reconstruction used an approximately uniform prior and the same flow architecture as our 2D experiment. We draw the following conclusions. (i) Flow-based models can represent complex 6D densities far from their unimodal base densities. All simulated measurements agree with the ground truth. Charged particle beams are often smooth and unimodal; therefore, we presume that flow-based models will be sufficient for most applications in accelerator physics. (ii) Some complex, high-dimensional distributions require large numbers of measurements to reconstruct with high precision. Of course, the required precision varies with application. In our case, the distribution’s primary features are largely determined from only 25 measurements in Fig. 3, but the entropy penalty eliminates unnecessary high-frequency terms in the distribution function. These terms are still present in the unregularized reconstruction when we quadruple the number of measurements in Fig. 4. (iii) MENT-Flow can scale to large measurement sets in reasonable time.

The Gaussian mixture distribution has little overlap between modes, so mismatch between the true and reconstructed distribution is obvious from low-dimensional views. This is not always the case. Direct measurements of low-energy hadron beams have unveiled hollow structures in high-dimensional phase space which are not evident in low-dimensional views.<sup>9</sup> This motivates us to test tomographic reconstruction algorithms on distributions with hidden internal structure. To this end, an  $n$ -dimensional “rings” distribution serves as the ground truth in Fig. 5-6; particles populate two concentric  $n$ -spheres with radii  $r_2 = 2r_1$ , and the radii are perturbed with Gaussian noise to generate a smooth density.

The entropy-regularized distribution maintains the spherical symmetry of the Gaussian prior, flattening and eventually inverting its radial density profile to fit the data.<sup>10</sup> The sliced views reveal an internal structure—

<sup>9</sup> Measurements at the Spallation Neutron Source (SNS) Beam Test Facility (BTF) [1] show space-charge-driven hollowing in 3D and 5D projections of the 6D phase space distribution.

<sup>10</sup> The one-dimensional projections in Figs. 5-6 are nearly Gaussian. Klartag [32] proved that almost all  $m$ -dimensional projections of an isotropic (no linear correlations)  $n$ -dimensional log-concave distribution function are nearly Gaussian when  $n \gg m$ . Many distributions commonly used in accelerator modeling are log-concave, such as the  $n$ -dimensional Gaussian, Waterbag (uniformly filled ball), and KV (uniformly filled sphere) distributions. A practical implication of this theorem is that small fluctuations in the  $m$ -dimensional projections have a greater impact on the  $n$ -dimensional reconstructed distribution as  $|n - m|$  increases—for instance, completely inverting the density profile from peaked to hollow. Thus, we found that later training epochs can significantly change the distribution while only slightly decreasing the loss function. It follows that, for certain distributions, there may be some value of  $|n - m|$  for which  $n:m$  tomography is practically impossible.

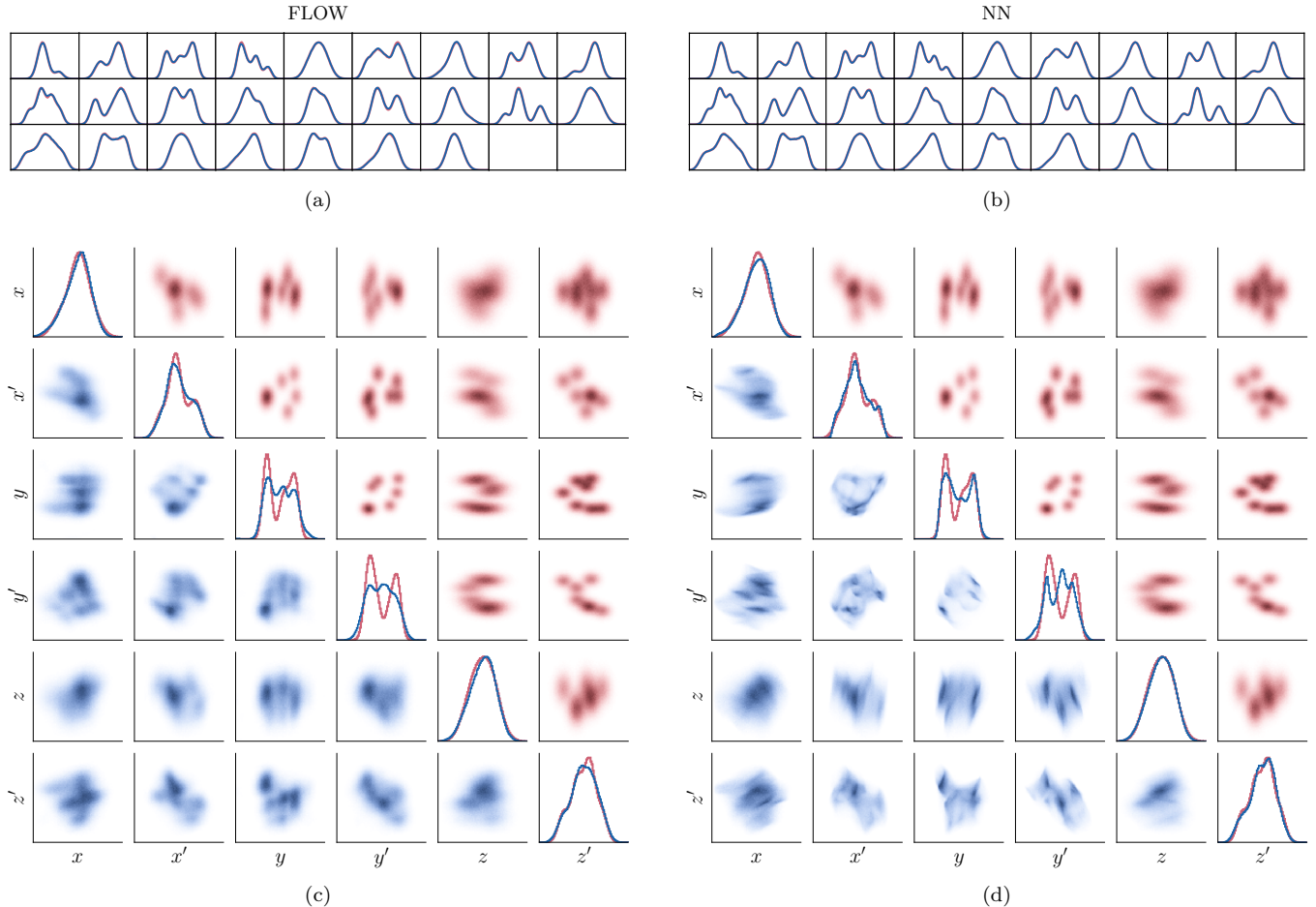


FIG. 3. Reconstruction of 6D Gaussian mixture distribution from 25 random 1D projections. (a-b) Simulated/true projections. (c-d) 1D/2D projections of reconstructed 6D distribution. Reconstructed/true 2D projections are plotted on the lower/upper triangular; 1D projections are overlaid on the diagonal.

a dense core surrounded by a low-density cloud—that is better approximated by MENT-Flow when measurements are scarce. In addition to injecting unnecessary correlations between planes, the unregularized solution ejects all particles from the core. Surprisingly, adding additional measurements does not solve the problem and generates two distinct modes in the reconstructed density. Using a different random seed to define the measurement axes can generate different patterns, but the hollowing and splitting just described are typical. Note that this internal structure is not obvious from the full 2D projections in the left column of Figs. 5-6. In experimental settings, we often have strong a priori assumptions of smoothness and unimodality based on beam dynamics simulations and theory. By encoding this background knowledge in MENT-Flow’s prior distribution, we are likely to obtain more reliable high-dimensional reconstructions.

#### IV. CONCLUSION AND EXTENSIONS

MENT-Flow is a promising approach to high-dimensional maximum-entropy phase space tomography. Numerical experiments demonstrate consistency with known 2D maximum-entropy solutions and the ability to fit complex 6D phase space distributions to large measurement sets. Our numerical experiments also emphasize the importance of regularization and uncertainty quantification in high-dimensional phase space tomography. We demonstrated that large numbers of 1D projections are insufficient to reconstruct certain complex 6D distributions with high precision. Future work should apply the method to more realistic distributions and phase space transformations. Additionally, future work should study the importance of entropy regularization when the measurements are 2D projections (which we expect to contain exponentially more information per measurement) or come from alternative diagnostics [33]. At the same time, alternative maximum-entropy algorithms should be investigated to address a wider range of prob-

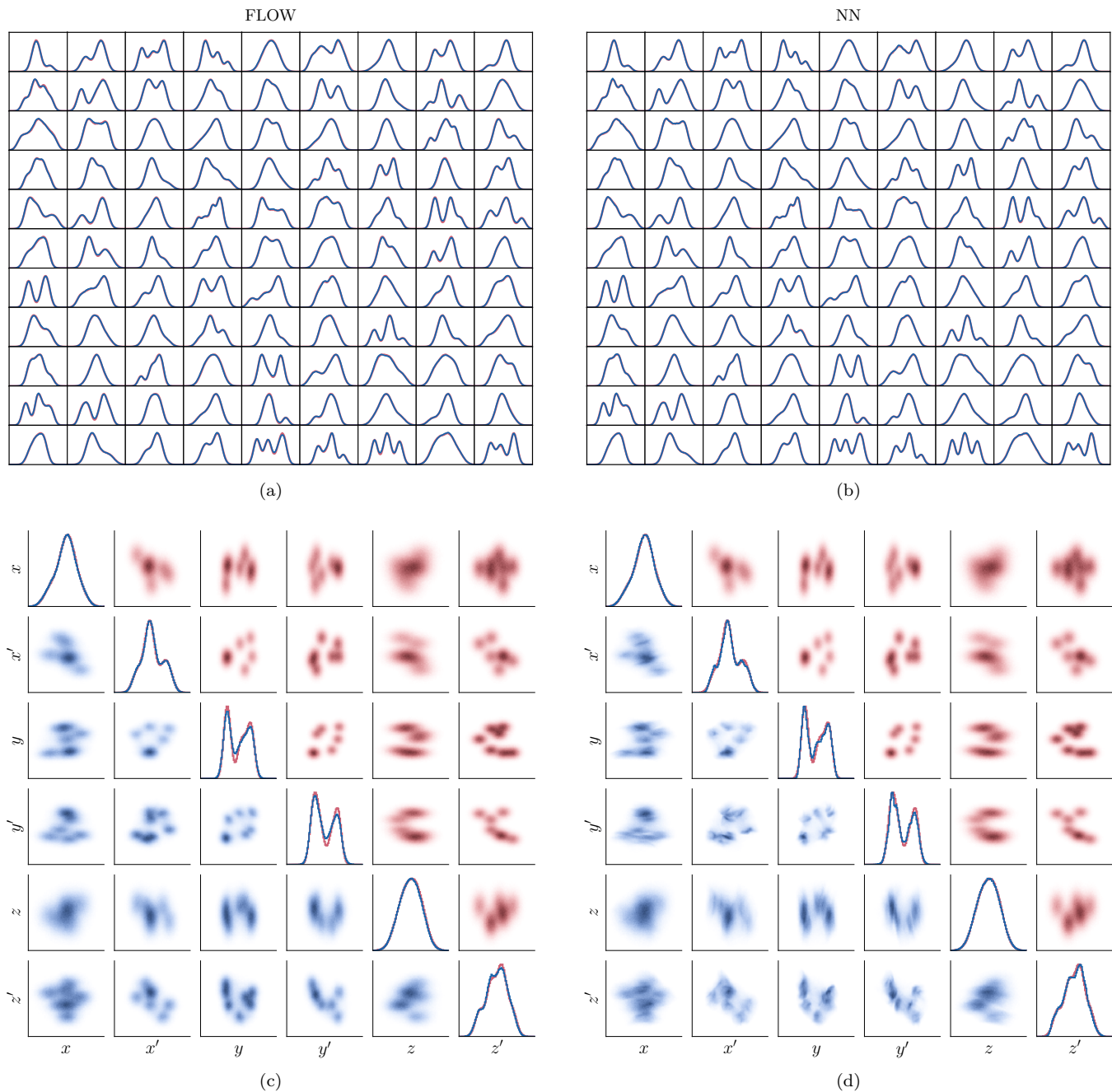


FIG. 4. Reconstruction of 6D Gaussian mixture distribution from 100 random 1D projections. (a-b) Simulated/true projections. (c-d) 1D/2D projections of reconstructed 6D distribution. Reconstructed/true 2D projections are plotted on the lower/upper triangular; 1D projections are overlaid on the diagonal.

lems.

MENT-Flow’s primary shortcomings are its slow sampling speed, its large number of parameters, and its restriction to differentiable particle dynamics. Sampling is approximately 50% slower than a conventional neural network, and the total runtime is increased by the need to solve multiple subproblems to approach the maximum-entropy distribution from below. This motivates the

search for even more efficient flows and sample-based entropy estimates. Note, however, that the total training time is already reasonable, ranging from 3 to 15 minutes on a single GPU in our experiments (depending on the number of projections, phase space dimension, batch size, and penalty parameter updates).

Flow-based phase space tomography may be able to approach maximum-entropy solutions to unexplored



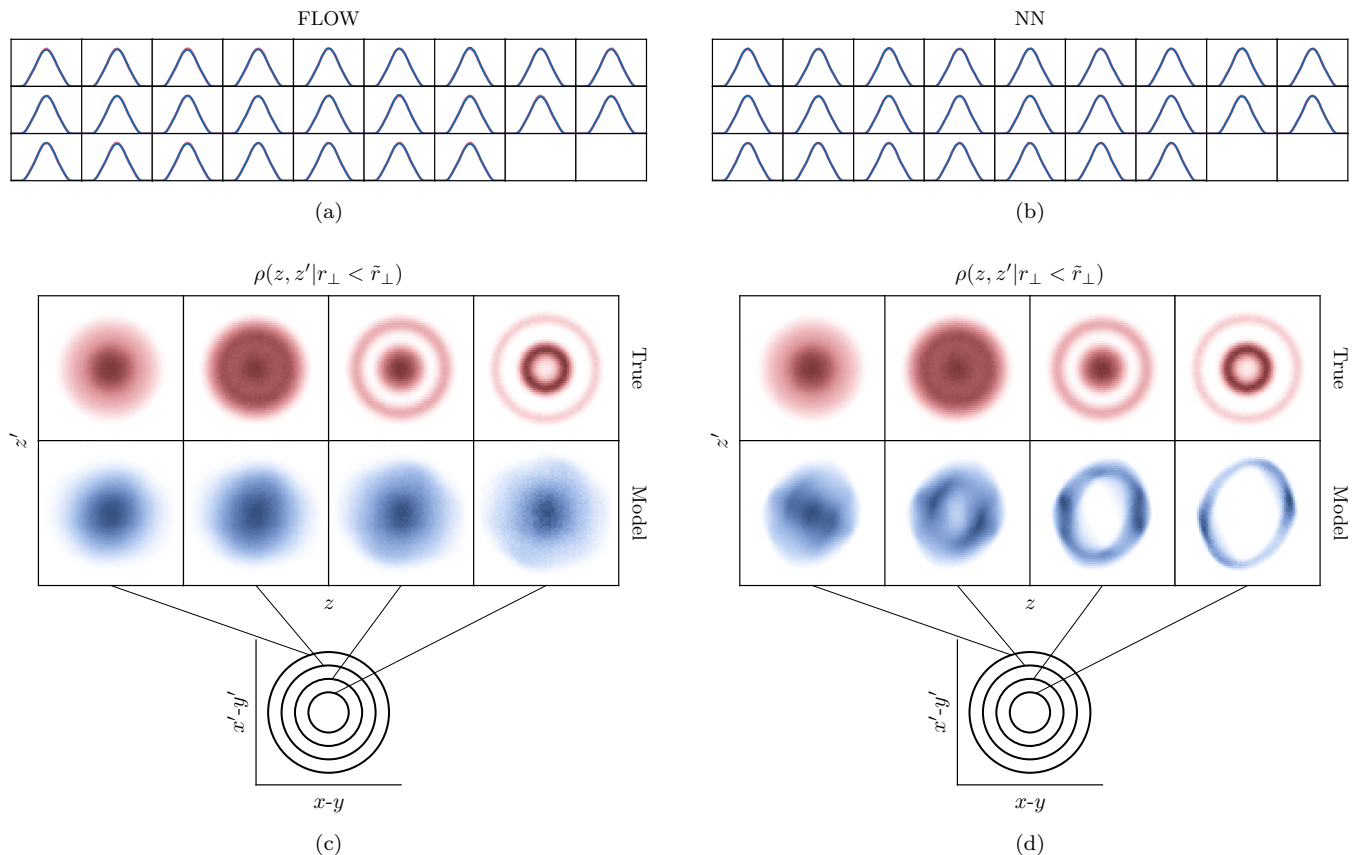


FIG. 5. Reconstruction of 6D “rings” distribution from 25 random 1D projections. (a-b) Simulated/true projections. (c-d) Reconstructed 2D projections within shrinking 4D ball of radius  $\tilde{r}_\perp = \sqrt{x^2 + x'^2 + y^2 + y'^2}$  in unplotted dimensions.

problems. First, MENT-Flow may be able to reconstruct  $n$ -dimensional distributions from high-dimensional projections ( $m > 2$ ). Such problems are of theoretical interest but also have some practical relevance. 3D and 4D projections can be measured relatively quickly using slit-screen-dipole measurement systems in low-energy hadron accelerators [1–3]. Projections may be *partial*, i.e., defined within a slice along other dimensions. The differentiable kernel density estimation needed to simulate the projections will perform poorly in these cases, so we propose to draw samples from the measured projections and minimize a statistical distance between these samples and samples from the flow.

Next, a particularly interesting application of maximum-entropy tomography is to intense hadron beams. Since space charge can generate highly nonlinear self-fields that depend on the 3D spatial distribution, knowledge of the full 6D phase space distribution is needed to predict the evolution of intense beams. A common measurement setup is to place the reconstruction location upstream of the measurement location, thereby allowing low-dimensional measurements under varying transport conditions (e.g. quadrupole scan) to obtain more information about the beam at the reconstruction point. Introducing transport renders the tomography

problem a significant challenge for intense beams because the forward process depends on self-fields of the unknown phase space distribution. With MENT-Flow, it may be possible to include space charge in the beam dynamics using differentiable space charge models [34]. We also plan to pursue tomography under intense space charge with conventional MENT, which may provide a benchmark for MENT-Flow results.

Finally, quantifying reconstruction uncertainty will be a crucial step for the operational use of high-dimensional phase space tomography. Of particular interest are Bayesian methods, where a prior probability is assigned to every possible phase space distribution and updated after observing the data. (The principle of maximum entropy claims that the prior should increase as a function of entropy [13], so the strategy in this paper remains correct if we must select a single distribution.) Several authors have used generative models to solve inverse image reconstruction problems via Bayesian posterior sampling [35]. Perhaps similar methods could be applied to our case.

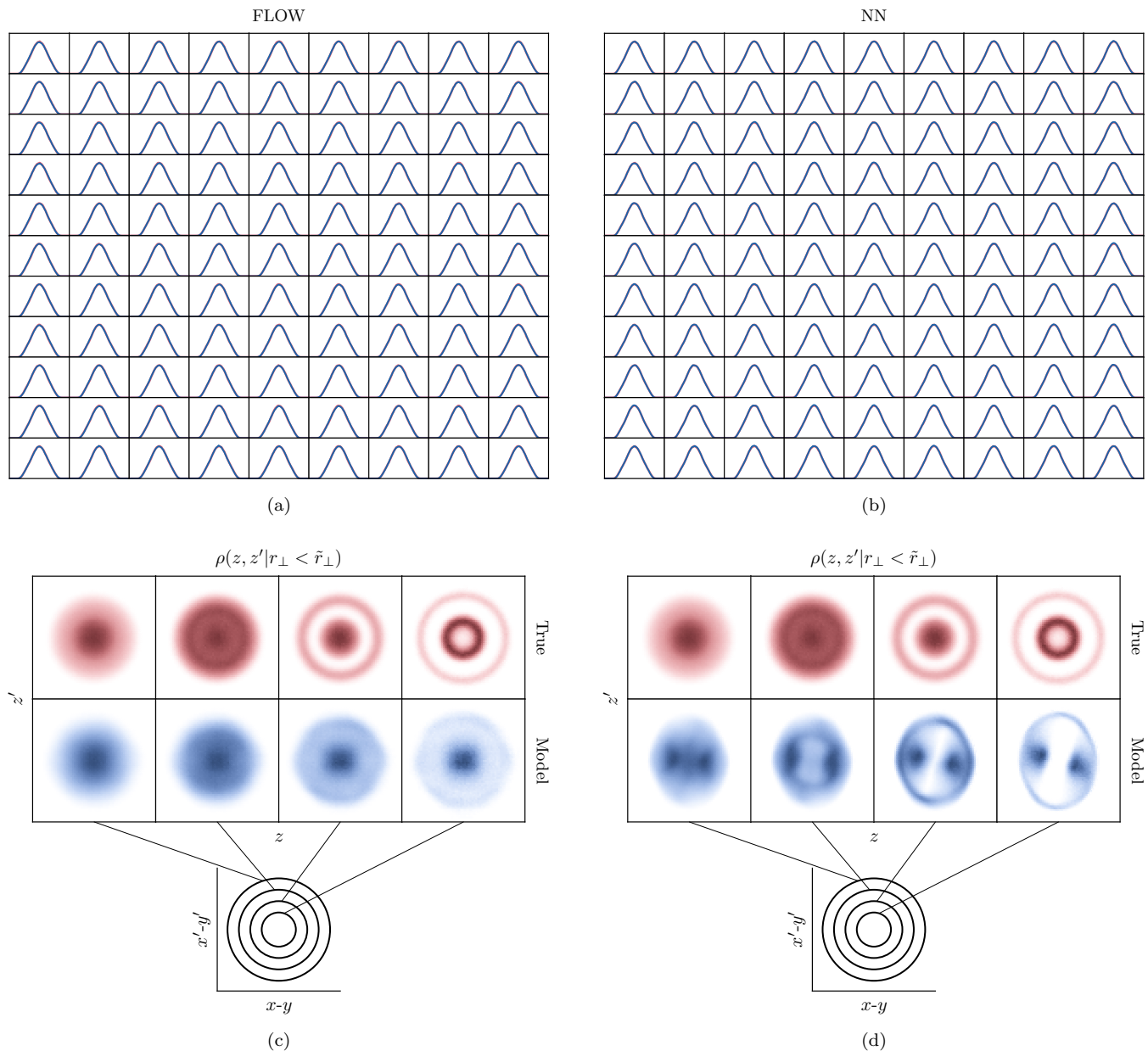


FIG. 6. Reconstruction of 6D “rings” distribution from 100 random 1D projections. (a-b) Simulated/true projections. (c-d) Reconstructed 2D projections within shrinking 4D ball of radius  $\tilde{r}_{\perp} = \sqrt{x^2 + x'^2 + y^2 + y'^2}$  in unplotted dimensions.

## V. ACKNOWLEDGEMENTS

We are grateful to Ryan Roussel (SLAC National Accelerator Laboratory), Juan Pablo Gonzalez-Aguilera (University of Chicago), and Auralee Edelen (SLAC National Accelerator Laboratory) for discussions that seeded the idea for this work and for sharing their differentiable kernel density estimation code.

This manuscript has been authored by UT Battelle, LLC under Contract No. DE-AC05-00OR22725 with the U.S. Department of Energy. The United

States Government retains and the publisher, by accepting the article for publication, acknowledges that the United States Government retains a non-exclusive, paid-up, irrevocable, world-wide license to publish or reproduce the published form of this manuscript, or allow others to do so, for United States Government purposes. The Department of Energy will provide public access to these results of federally sponsored research in accordance with the DOE Public Access Plan (<http://energy.gov/downloads/doe-public-access-plan>).

- 
- [1] B. Cathey, S. Cousineau, A. Aleksandrov, and A. Zhukov, First six dimensional phase space measurement of an accelerator beam, *Phys. Rev. Lett.* **121**, 064804 (2018).
- [2] K. Ruisard, A. Aleksandrov, S. Cousineau, V. Tzoganis, and A. Zhukov, High dimensional characterization of the longitudinal phase space formed in a radio frequency quadrupole, *Phys. Rev. Accel. Beams* **23**, 124201 (2020).
- [3] A. Hoover, K. Ruisard, A. Aleksandrov, A. Zhukov, and S. Cousineau, Analysis of a hadron beam in five-dimensional phase space, *Phys. Rev. Accel. Beams* **26**, 064202 (2023).
- [4] K. Hock and A. Wolski, Tomographic reconstruction of the full 4d transverse phase space, *Nuclear Instruments and Methods in Physics Research Section A: Accelerators, Spectrometers, Detectors and Associated Equipment* **726**, 8 (2013).
- [5] M. Wang, Z. Wang, D. Wang, W. Liu, B. Wang, M. Wang, M. Qiu, X. Guan, X. Wang, W. Huang, and S. Zheng, Four-dimensional phase space measurement using multiple two-dimensional profiles, *Nuclear Instruments and Methods in Physics Research Section A: Accelerators, Spectrometers, Detectors and Associated Equipment* **943**, 162438 (2019).
- [6] A. Wolski, D. C. Christie, B. L. Militsyn, D. J. Scott, and H. Kockelbergh, Transverse phase space characterization in an accelerator test facility, *Phys. Rev. Accel. Beams* **23**, 032804 (2020).
- [7] J. C. Wong, A. Shishlo, A. Aleksandrov, Y. Liu, and C. Long, 4d transverse phase space tomography of an operational hydrogen ion beam via noninvasive 2d measurements using laser wires, *Physical Review Accelerators and Beams* **25**, 10.1103/PhysRevAccelBeams.25.042801 (2022).
- [8] A. Scheinker, F. Cropp, and D. Filippetto, Adaptive autoencoder latent space tuning for more robust machine learning beyond the training set for six-dimensional phase space diagnostics of a time-varying ultrafast electron-diffraction compact accelerator, *Phys. Rev. E* **107**, 045302 (2023).
- [9] A. Wolski, M. A. Johnson, M. King, B. L. Militsyn, and P. H. Williams, Transverse phase space tomography in an accelerator test facility using image compression and machine learning, *Phys. Rev. Accel. Beams* **25**, 122803 (2022).
- [10] S. Jaster-Merz, R. Assmann, R. Brinkmann, F. Burkart, W. Hillert, M. Stanitzki, and T. Vinatier, 5d tomographic phase-space reconstruction of particle bunches, *arXiv preprint arXiv:2305.03538* (2023).
- [11] R. Roussel, A. Edelen, C. Mayes, D. Ratner, J. P. Gonzalez-Aguilera, S. Kim, E. Wisniewski, and J. Power, Phase space reconstruction from accelerator beam measurements using neural networks and differentiable simulations, *Physical Review Letters* **130**, 145001 (2023).
- [12] R. Roussel, J. P. Gonzalez-Aguilera, A. Edelen, E. Wisniewski, A. Ody, W. Liu, Y.-K. Kim, and J. Power, Efficient 6-dimensional phase space reconstruction from experimental measurements using generative machine learning (2024).
- [13] J. Skilling and S. F. Gull, Bayesian maximum entropy image reconstruction, *Lecture Notes-Monograph Series*, 341 (1991).
- [14] S. Pressé, K. Ghosh, J. Lee, and K. A. Dill, Principles of maximum entropy and maximum caliber in statistical physics, *Rev. Mod. Phys.* **85**, 1115 (2013).
- [15] R. D. Rosenkrantz, *ET Jaynes: Papers on probability, statistics and statistical physics*, Vol. 158 (Springer Science & Business Media, 2012).
- [16] G. Loaiza-Ganem, Y. Gao, and J. P. Cunningham, Maximum entropy flow networks, in *International Conference on Learning Representations* (2016).
- [17] G. Minerbo, Ment: A maximum entropy algorithm for reconstructing a source from projection data, *Computer Graphics and Image Processing* **10**, 48 (1979).
- [18] C. T. Mottershead, Maximum entropy tomography (1996).
- [19] N. J. Dusaussouy and I. E. Abdou, The extended ment algorithm: a maximum entropy type algorithm using prior knowledge for computerized tomography, *IEEE Transactions on Signal Processing* **39**, 1164 (1991).
- [20] A. Tran and Y. Hao, Beam tomography with coupling using maximum entropy technique, in *Proc. 14th International Particle Accelerator Conference, IPAC'23 - 14th International Particle Accelerator Conference No. 14* (JACoW Publishing, Geneva, Switzerland, 2023) pp. 3944–3947.
- [21] S. Basir and I. Senocak, An adaptive augmented lagrangian method for training physics and equality constrained artificial neural networks, *arXiv preprint arXiv:2306.04904* (2023).
- [22] Z. Ao and J. Li, Entropy estimation via normalizing flow, in *Proceedings of the AAAI Conference on Artificial Intelligence*, Vol. 36 (2022) pp. 9990–9998.
- [23] V. Stimper, B. Schölkopf, and J. M. Hernández-Lobato, Resampling base distributions of normalizing flows, in *Proceedings of the 25th International Conference on Artificial Intelligence and Statistics (AISTATS)*, Proceedings of Machine Learning Research, Vol. 151 (PMLR, 2022) pp. 4915–4936.
- [24] G. M. Green, Y.-S. Ting, and H. Kamdar, Deep potential: Recovering the gravitational potential from a snapshot of phase space, *The Astrophysical Journal* **942**, 26 (2023).
- [25] C. Durkan, A. Bekasov, I. Murray, and G. Papamakarios, Neural spline flows, *Advances in neural information processing systems* **32** (2019).
- [26] G. Papamakarios, T. Pavlakou, and I. Murray, Masked autoregressive flow for density estimation, *Advances in neural information processing systems* **30** (2017).
- [27] A. Hoover, Ment-flow: maximum-entropy phase space tomography using normalizing flows, 10.5281/zenodo.11406452 (2024).
- [28] A. Aleksandrov, S. Cousineau, and K. Ruisard, Understanding beam distributions in hadron linacs in the presence of space charge, *Journal of Instrumentation* **15** (7), P07025.
- [29] M. Laszkiewicz, J. Lederer, and A. Fischer, Marginal tail-adaptive normalizing flows, in *Proceedings of the 39th International Conference on Machine Learning*, Proceedings of Machine Learning Research, Vol. 162, edited by K. Chaudhuri, S. Jegelka, L. Song, C. Szepesvari, G. Niu, and S. Sabato (PMLR, 2022) pp. 12020–12048.
- [30] V. A. Lebedev and S. Bogacz, Betatron motion with coupling of horizontal and vertical degrees of freedom, *Jour-*

- nal of Instrumentation **5** (10), P10010.
- [31] B. Dai and U. Seljak, Sliced iterative normalizing flows, in *Proceedings of the 38th International Conference on Machine Learning*, Proceedings of Machine Learning Research, Vol. 139, edited by M. Meila and T. Zhang (PMLR, 2021) pp. 2352–2364.
- [32] B. Klartag, A central limit theorem for convex sets, *Inventiones mathematicae* **168**, 91 (2007).
- [33] K. Hwang, C. Mitchell, and R. Ryne, Machine learning based phase space tomography using kicked beam turn-by-turn centroid data in a storage ring, *Phys. Rev. Accel. Beams* **26**, 104601 (2023).
- [34] J. Qiang, Differentiable self-consistent space-charge simulation for accelerator design, *Phys. Rev. Accel. Beams* **26**, 024601 (2023).
- [35] M. Mardani, J. Song, J. Kautz, and A. Vahdat, A variational perspective on solving inverse problems with diffusion models, arXiv preprint arXiv:2305.04391 (2023).